Analytica Chimica Acta 1397 (2026) 345285

Contents lists available at ScienceDirect

Analytica Chimica Acta

journal homepage: www.elsevier.com/locate/aca

Faster, simpler, and more precise calibration curves: Expanding the scope of continuous calibration

Peter J.H. Williams *, Nadini Thushara, Amin Yousefi, Harrison Mundschutz, Dennis K. Hore, J. Scott McIndoe **

Department of Chemistry, University of Victoria, PO Box 1700 STN CSC, Victoria, BC, V8W 2Y2, Canada

HIGHLIGHTS

- The continuous calibration method was expanded, simplified, and demonstrated.
- Molar absorption coefficients were determined from a single experiment.
- The literature pK_a of a weak acid was obtained from a single experiment.

GRAPHICAL ABSTRACT

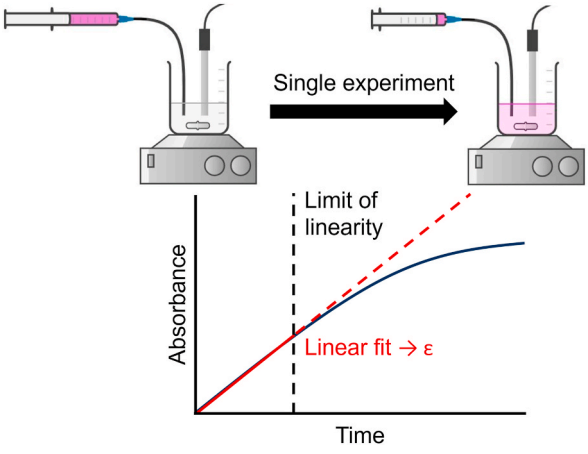

ARTICLE INFO

Handling Editor: Prof. L. Buydens

ABSTRACT

Background: Accurate calibration curves are essential for quantitative analysis but are often neglected due to their time, cost, and labour demands. Traditional calibration involves measuring solutions of known concentrations to construct a calibration curve relating analyte concentration to instrument response. While these relationships rarely follow simple closed-form equations, linear approximations are commonly used for simplicity, often being fitted with too few data points for high-accuracy calibration. Continuous calibration addresses these challenges by continuously infusing concentrated calibrant into a clean matrix solution while monitoring the response online. This approach significantly reduces time and labour while generating extensive data, improving calibration precision and accuracy. Despite its advantages, method limitations and technical complexities have hindered widespread adoption.

Results: Here, continuous calibration is expanded and simplified with modern accessible equipment, open-source code, and a user-friendly web tool that together streamline experiments and data processing. The software generates smoothed and equation-fitted calibration curves complete with statistical-validity, quality-of-fit, and

* Corresponding author.
** Corresponding author.
E-mail addresses: peterwilliams@uvic.ca (P.J.H. Williams), mcindoe@uvic.ca (J.S. McIndoe).

https://doi.org/10.1016/j.aca.2026.345285
Received 17 November 2025; Received in revised form 2 February 2026; Accepted 20 February 2026
Available online 20 February 2026

dynamic-range estimates. The method was demonstrated over a broad range of systems and analytical techniques, including external, standard addition, and internal standardization calibrations, and mass spectrometry, and infrared and ultraviolet–visible spectroscopies. The technique was also demonstrated to be more efficient and precise than discrete calibration. In ultraviolet–visible applications, molar absorption coefficients (ε) were obtained from a single experiment, with values for multiple analytes matching literature. For example, $KMnO_4$/H_2O analysis yielded $\varepsilon = 2450 \pm 40$ M^{-1} cm^{-1} compared to the reported 2250–3340 M^{-1} cm^{-1}. The approach was further extended to calibrate instrument response across pH ranges, yielding the literature pK_a of a weak acid from a single experiment.

Significance: These advancements substantially improve the precision, efficiency, and accessibility of calibration, with the potential to enhance experimental quality and efficiency across many fields. We hope that these improvements encourage scientists to conduct high-quality calibration more frequently.

1. Introduction

Accurate calibration, for relating observed analyte intensity to its concentration, is essential for quantitative analysis, for example in sample analysis and kinetic studies [1–4]. In particular, modern kinetic techniques such as reaction progress kinetic analysis and continuous addition kinetic elucidation rely on precise quantification to extract kinetic parameters and mechanistic conclusions from continuously collected spectral data [5–7].

Traditional external calibration involves measuring several solutions of known concentrations to create a calibration curve relating analyte concentration to instrument response. Matrix-matched calibration improves this method by calibrating with a matrix similar to the sample matrix. Similarly, standard addition involves incrementally spiking a sample with a calibrant solution of known concentration and measuring instrument response to estimate the original sample concentration. Internal standardization instead employs a reference species of known concentration that behaves similarly to the analyte [1–3,8].

The relationship between concentration and instrument response can rarely be described by simple closed-form equations [9]. Factors including analyte properties, the sample matrix, and instrument parameters often unpredictably influence calibration [10–16]. Moreover, instruments rarely have long-term stability and often have poor short-term stability, necessitating frequent recalibration for high-accuracy measurements [4,17]. Despite these complexities, linear approximations are frequently used for simplicity, particularly at lower concentration ranges where greater linearity is often observed [3,9]. However, calibrations with few data risk the inappropriate application of linear fits, leading to inaccuracies [18]. While high-quality calibration is critical, it is often neglected due to the time, cost, and labour required for preparing and measuring multiple solutions of known concentration [4,19,20]. This compromise ultimately degrades experiment result quality. Therefore, simplifying and expediting calibration is essential to improve analysis and promote better scientific practices.

Several techniques aim to address these challenges. Automated discrete calibration methods, such as automated dilution and flow-injection analysis [21], reduce manual effort. However, like other discrete calibration techniques, they are limited by the small number of data points they generate. Additionally, they often require specialized instrumentation. One alternative technique utilized an ever-increasing flow of concentrated calibrant solution mixed with aspirated solvent to create a continuously increasing concentration of calibrant, which was infused into a continuously monitoring atomic absorption spectrometer [22]. Continuous calibration is a different approach which instead continuously infuses concentrated calibrant solution into a clean matrix solution monitored online direct detection. Both techniques significantly reduce labour and time while generating numerous data, thereby improving calibration accuracy. Continuous calibration was first developed for use in atomic absorption spectroscopy, where non-linear calibration curves were used for interpolating sample intensities to concentration [23]. It was later adapted for inductively coupled plasma (ICP) atomic emission spectrometry and ICP mass spectrometry (MS), using linear fits to convert sample intensities into concentrations [24,25]. These studies demonstrated that continuous calibration outperformed conventional calibration techniques in speed, efficiency, and precision [24]. The nature of these spectrometric techniques means that discrete calibration is especially time consuming and hence they greatly benefit from the efficacy of continuous calibration. However, these methods relied on Mariotte's bottles and peristaltic pumps, which can be expensive, restrictive, incompatible with certain solvents, and require large volumes of calibrant solution. These limitations, coupled with uncertainties and complexities of data handling, have hindered widespread adoption amongst other analytical techniques.

Here, continuous calibration is simplified, expanded, and applied to a broader array of systems and analytical techniques. Analyte is infused using a syringe pump, which is more cost-effective and widely available than the previously used equipment. A web application (http://www.catacycle.com/cc) streamlines data processing by allowing users to upload calibration data to generate smoothed and equation-fitted calibration curves, complete with quality-of-fit estimates and dynamic range estimates. Users can also upload experimental intensity data to calculate their corresponding concentrations through application of continuous calibration curves. The tool includes algorithms for statistical validation of linear and non-linear fits and estimation of the maximum accurately quantifiable concentration. For more advanced applications, the underlying code is freely available for offline use and modification, such as fitting to custom equations (https://github.com/peterjhw07/continuous_calibration). The method was demonstrated for external, standard addition, and internal standardization calibration curves. It was also successfully applied to electrospray ionization (ESI) MS, and infrared (IR) and ultraviolet–visible (UV–Vis) spectroscopies, with the latter enabling molar absorption coefficients to be calculated from a single experiment. By reducing time and labour and increasing calibration precision, this approach and the improvements described herein have the potential to enhance experimental efficiency and result accuracy across multiple fields.

Calibration curves are also key to quantification of chromatographic-coupled techniques, such as liquid chromatography MS (LC-MS). Continuous calibration cannot be applied to such methods, presenting a key limitation. It is not immediately obvious how this could be overcome, particularly due to complications regarding analyte spread and solvent gradients. Overcoming these limitations would further expand the applications of continuous calibration and greatly benefit the analytical community, though is beyond the scope of this manuscript.

2. Experimental

In continuous calibration, a syringe pump was used to infuse an addition solution into a stirred flask of monitored solution. All species in the addition solution were of known concentration. The initial compositions of the monitored and addition solutions varied depending on the specific continuous calibration technique being employed (Table 1).

The monitored solution was measured using online direct detection either *in situ* (UV–Vis and IR spectroscopies) or *ex situ* via pressurized sample infusion (MS), without chromatographic separation [26,27].

Table 1
Initial matrix compositions of the monitored and addition solutions for each continuous calibration technique, excluding pH-modulating species and solvent.

Continuous calibration technique	Monitored solution species	Addition solution species
External	-	Analyte
Standard addition	Analyte	Analyte
Internal standardization	Internal standard	Analyte and internal standard
pH	Analyte (at first pH)	Analyte (at second pH)

Mass spectrometer parameters were automatically optimized via Bayesian optimization algorithms using OptiMS software [15]. Spectral acquisition was usually initiated before the continuous infusion of the addition solution commenced. Relevant analyte and internal standard peak intensities were extrapolated from spectra. The resultant time vs. intensity data were processed using open-source Python code (https://github.com/peterjhw07/continuous_calibration) that employed multiple packages [28–38]. The code uses the initial monitored solution volume, concentrations of analytes in the addition solution, and addition solution flow rate to calculate analyte concentrations over time. The resulting concentration vs. intensity data are then used to create data-dense calibration curves. The code also offers a variety of other functions to facilitate data manipulation and curve fitting. Once fitted, continuous calibration curves can be applied to discretely measured samples to predict analyte concentrations from their signal intensities. All uncertainties reported herein are standard errors unless otherwise specified. Full experimental details are provided in the Supporting Information.

3. Results and discussion

The continuous calibration method was principally developed using $KMnO_4$, dissolved in H_2O and monitored using UV–Vis spectroscopy, as a model calibrant due to its simplicity and ubiquity. First, conditions were optimized to ensure rapid diffusion occurred, using discrete increments of addition solution. This was essential to maximize continuous calibration accuracy. The optimized conditions yielded complete diffusion in <5 s (Fig. S4).

Once conditions were optimized, discrete and continuous $KMnO_4$ calibrations were performed in triplicate in a 0.00–1.20 mM concentration range. The resulting continuous calibration data showed excellent congruency with each other and the discrete calibration points (Fig. 1). The triplicate discrete data took ~10 h to collect, required measurement of 54 samples, and yielded 54 data points (~5.4 data points per hour). In contrast, the triplicate continuous data took ~1.75 h to collect with data acquisition occurring over 21 min each (Fig. S5), required measurements of three solutions, and yielded 3626 data points (~2100 data points per hour). This demonstrated that continuous calibration could be used to collect calibration data with the same accuracy as discrete calibration but more rapidly and with much greater density. Notably, the obtained calibration curves visually demonstrated non-linear behaviour (Fig. 1), as expected at high concentration values and absorbances.

This increased data density afforded by continuous calibration allowed more precise calibration curves to be constructed than possible for discrete calibration. The data were sufficiently dense that they could be used to create highly precise calibration curves without specific models. Alternatively, models could be used to fit an equation to the calibration curve for a particular concentration range, as is commonly executed using a linear function for discrete calibration data.

Algorithms, such as the rainbow test, were implemented into the code to determine a region in which a linear model was valid and hence estimate a limit of linearity. The null hypothesis of this test states that the difference between the fit of a linear model on a dataset compared to a central subset of the dataset is insignificant [39]. The code iteratively

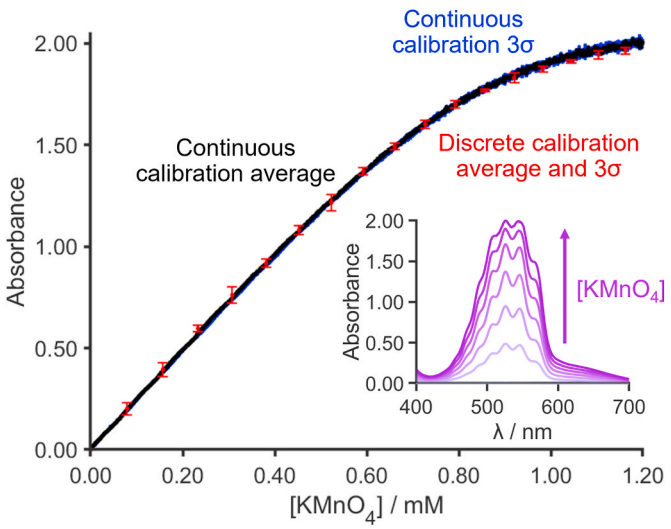

Fig. 1. Main) Averaged triplicate continuous calibration curves (black scatter) and the associated 3 × standard deviation (3σ) area (blue), compared with averaged triplicate discrete data and their associated 3σ (red), of $KMnO_4/H_2O$ monitored with UV–Vis spectroscopy. The high data density, low standard deviations, and close overlap with discrete data demonstrate the high precision and accuracy of continuous calibration. Inset) Corresponding UV–Vis spectra of one continuous calibration curve at each 0.20 mM interval.

performed the test between concentration zero and each concentration point. The maximum limit of linearity was determined to be the last data range for which the p value was above the set threshold ($p = 0.05$). This yielded a limit of linearity of 0.24 ± 0.04 mM across the three continuous calibration curves. This limit was notably less than the 0.86 mM limit of linearity determined from the discrete calibration data (Fig. S6). This was due to the greater data density measured during continuous calibration and the correspondingly greater curve definition provided by it, making deviation from linearity more apparent both visually and statistically. For example, the average root mean squared error (RMSE) across the three continuous calibration curves was 0.00326, much lower than the 0.0541 RMSE obtained from the discrete data.

From this linear relationship, the molar absorption coefficient (ε) was estimated to be 2450 ± 40 M^{-1} cm^{-1} (λ_{max} ~526 nm). This value was comfortably within the 2250–3340 M^{-1} cm^{-1} range reported in literature [40–44]. In contrast, ε was estimated from the discrete data to be 2230 ± 40 M^{-1} cm^{-1}, slightly below the literature range. This underestimation was caused by the inclusion of higher concentration points which deviated from linearity with a negative curvature (Fig. S6). This demonstrated that increased data density could improve calibration curve accuracy through enhanced precision.

Alternatively, the code can be used to maximize the coefficient of determination (R^2). This obtained a limit of linearity of 0.33 ± 0.02 mM and ε = 2430 ± 40 M^{-1} cm^{-1} (λ_{max} ~526 nm) across the three continuous calibration curves, closely agreeing with the previously determined value. While this test does not algorithmically justify the use of a linear equation, it more closely resembles linear fitting of conventional discrete calibration curves and usually yields wider limits of fitting. Consistently, maximizing R^2 for the discrete data yielded a limit of fitting of 0.38 mM and ε = 2460 ± 30 M^{-1} cm^{-1}, which was within the literature range. However, the limit of fitting was again seemingly overestimated, and the RMSE (0.00409) was lower than for the continuous data (average of 0.00352). Together, these observations demonstrated that continuous calibration was more robust than discrete calibration.

While calibration curves are most frequently fit using linear equations, they can also be fit using non-linear models (Table S3). As for linear fitting, fitting using discrete non-linear equations necessitated a

limit of fitting to be determined. For this, an algorithm was implemented to determine the region of maximum R^2 and hence estimate a limit of fitting, iteratively performing analysis between concentration zero and each concentration point. Higher qualities of fit across wider concentration ranges were yielded using logarithmic (0.00–0.50 ± 0.01 mM, R^2 = 0.99993 ± 0.00001) and tangential functions (0.00–0.62 ± 0.01 mM, R^2 = 0.99995 ± 0.00001) than a linear function (0.00–0.33 ± 0.02 mM, R^2 = 0.99975 ± 0.00004), increasing the calibrated region and therefore useable concentration range. Alternatively, generalized additive models (GAMs), could be used to construct high-quality calibration curves without the need for easily interpretable equations. The high data density afforded by continuous calibration results in GAMs having high accuracy. For the $KMnO_4/H_2O$ continuous calibration, a concave GAM yielded a high R^2 across the whole concentration range (0.00–1.20 mM, R^2 = 0.99991 ± 0.00001). All these and further options are available through the code and web application. Examples of these fits for one of the continuous calibration experiments are shown below (Fig. 2).

From fitted curves, the code also determines the limit of detection, estimated as the concentration corresponding to 3 × the standard deviation of measured blank solution intensities. For example, the limit of detection calculated for the linear fits was 0.0021 ± 0.0002 mM. Alternatively, more rigorous methods for determining the limit of detection could be applied to repeated calibration curves [45].

As observed previously, the discrete data yielded greater limits of fitting for all functions than the continuous data (Fig. S7). Furthermore, the data density of the continuous calibration curves afforded model coefficients with significantly lower standard errors than the discrete data (Table S4). For example, the linear model fitted to the discrete data produced a gradient of 2460 ± 30 mM^{-1}, compared to an average gradient and standard error of 2433 ± 1 mM^{-1} from the continuous data. These results demonstrated that continuous calibration produced curves of greater precision, and therefore higher confidence, than discrete calibration.

Once fitted, continuous calibration curves can be applied to predict analyte concentrations in discretely measured samples from their signal intensities. This can be performed using the code and web application. To demonstrate such application, the fitted curves were used to validate the concentrations of the 54 discretely measured triplicate samples. The predicted concentrations closely matched the known values, up to the limit of fitting of each function (Table S5–6). For example, for the 0.308 ± 0.005 mM samples, the linear-, logarithmic-, tangential-, and GAM-fitted continuous calibration curves predicted concentrations of 0.313 ± 0.009, 0.316 ± 0.009, 0.315 ± 0.009, and 0.315 ± 0.009 mM respectively; recoveries of 102–103 ± 1%. Average recoveries within the limits of fitting were 104 ± 1%, 103 ± 1%, 102 ± 1%, and 100 ± 1%, demonstrating high accuracy and precision. Comparable average recoveries of 103 ± 1%, 100 ± 1%, 100 ± 1%, and 106 ± 3% were observed for the discrete data using leave-one-out cross-validation (Table S8). Notably, the GAM performed poorly, achieving lower accuracy and precision than its continuous counterpart, especially at lower concentrations. This was due to the high number of data required to fit GAMs accurately.

For both continuous and discrete calibration curves, prediction accuracy deteriorated above the limits of fitting, as expected (Table S5–8). For instance, for the 0.73 ± 0.01 mM samples, the linear-, logarithmic-, tangential-, and GAM-fitted continuous calibration curves predicted concentrations of 0.66 ± 0.02 (90 ± 3% recovery), 0.69 ± 0.02 (95 ± 3% recovery), 0.71 ± 0.02 (97 ± 3% recovery), and 0.73 ± 0.02 mM (100 ± 3% recovery) respectively, with only the GAM having a limit of fitting above the sample concentrations. The higher the concentration was above the limit of fitting the worse the predictive accuracy became. This further demonstrated that linear models produced narrower limits

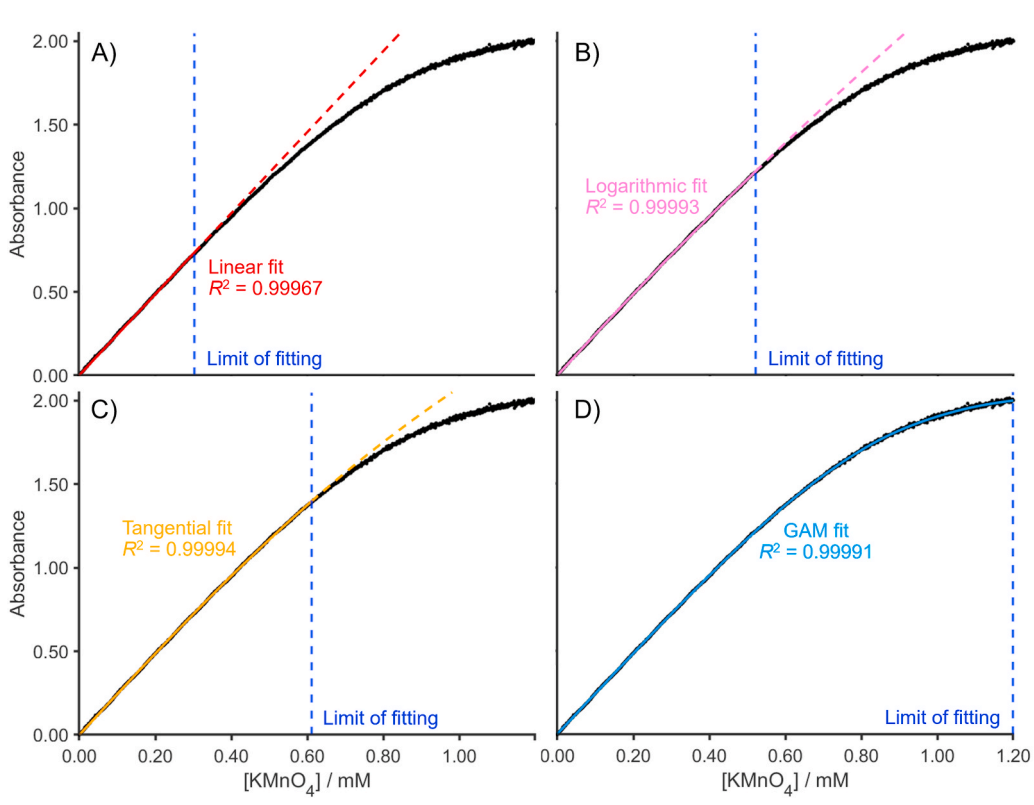

Fig. 2. Fitting of different functions to a continuous calibration of a $KMnO_4/H_2O$ system, monitored with UV–Vis spectroscopy. Depicted are experimental data (black scatter) and fits with algorithmically determined limits of fitting (dashed dark blue line) which maximized R^2 (solid coloured lines) and continuation of the fits beyond the limits of fitting (dashed coloured lines). The fits use A) linear (red), B) logarithmic (pink), C) tangential (orange), and D) generalized additive model (GAM) functions (light blue).

of quantification than non-linear models.

The continuous calibration method was extended to perform standard addition calibration. Standard addition calibration is significantly more time consuming and laborious than external calibration and internal standardization, as it requires a calibration curve to be constructed for each individual sample [46,47]. This technique will therefore benefit most from the faster and simpler continuous calibration approach. Continuous standard addition calibration was demonstrated using the continuous addition of a standard to a 0.157 ± 0.006 mM sample. This did not require nor use the continuous calibration curves built previously. Linear fitting, with a limit of linearity algorithmically determined at the last concentration which passed the runs test *p* value (a relatively strict equation fitting test), yielded an initial sample concentration of 0.161 ± 0.004 mM (Fig. 3) with a recovery of 103 ± 5%. This demonstrated that continuous calibration could be used to apply calibration curves and perform standard addition more efficiently and precisely than discrete calibration, greatly benefiting standard addition calibration.

For samples with unknown or irreproducible matrices, relative changes in the monitored solution volume should be minimized. This can be achieved by increasing the analyte concentration in the addition solution and by either increasing the initial monitored solution volume, decreasing the addition solution flow rate, or both. Alternatively, continuous standard dilution analysis is more robust to matrix alteration than continuous standard addition [48–51]. However, this method has other limitations, such as rate of concentration change decreasing as calibration progresses, leading to an uneven distribution of calibration data density.

The continuous calibration method was applied to additional analytes in an array of matrices. The close agreement between molar absorption coefficients measured through continuous calibration and physicochemically-similar literature systems demonstrated the robustness of the method across a range of conditions (Table 2). Additionally, a $[Ni_2(cage)]^{2+}$ complex [52] has its molar absorption coefficient measured for the first time using continuous calibration (Table 2). These experiments demonstrated that a molar absorption coefficient could be measured using a single continuous calibration experiment, reducing time and labour.

Beyond the improvements to calibration, the greater precision offered by the continuous alteration methods compared to discrete methods offer non-calibration benefits. For example, bathochromic and hypsochromic shifts were detected in many of the systems above (Table 2). These shifts indicate complex intramolecular interactions between species. For example, in rhodamine B, a hypsochromic shift was observed between ~11 and 30 μM from 552 nm to 547 nm (Fig. S8A). This hypsochromic shift corresponds with an approximately linear intensity increase of a convoluted peak with λ_{max} ~515 nm (Fig. S8B), attributed to H-aggregated dimer [67–69]. This demonstrated that continuous calibration can be used to precisely map the formation of intramolecular complexes across data-dense concentration ranges.

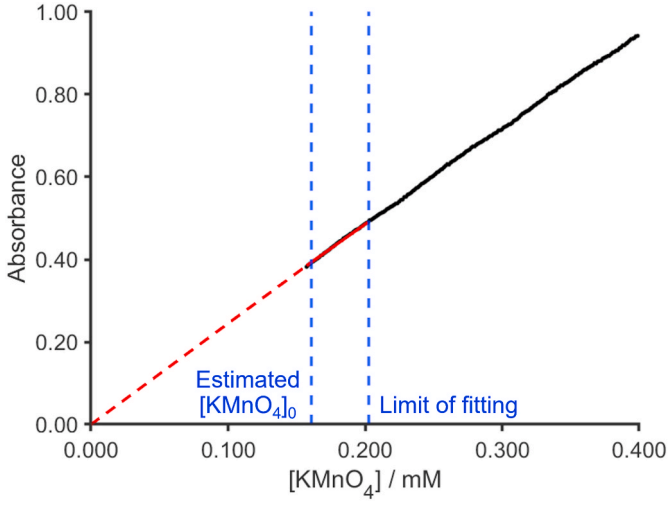

Fig. 3. Continuous standard addition calibration of a $KMnO_4/H_2O$ system to a 0.157 ± 0.006 mM sample monitored with UV–Vis spectroscopy. Depicted are experimental data (black scatter) and a linear fit (solid red line) with algorithmically determined limit of fitting (upper dashed blue line) which last passed the runs test *p* value (solid red line) and continuation of the fit below the limits of fitting (dashed red line), yielding an estimated concentration of 0.161 ± 0.004 mM (lower dashed blue line).

Table 2
Molar absorption coefficients measured using continuous calibration compared to literature values of physicochemically-similar systems. Limits of fitting were determined using the rainbow test. Errors were estimated from equipment and fitting uncertainties unless stated otherwise.

System	Modal measured λ_{max}/nm	Measured ε/M^{-1} cm^{-1}	Literature ε /M^{-1} cm^{-1}
$KMnO_4/H_2O$	525	2450 ± 40[a]	2250–3340[40–44]
Benzophenone/ MeOH	256	16300 ± 200	15100–19400 [53–55]
$CuSO_4/H_2O$	770	10.9 ± 0.3	12.3[56]
Ferrocene/$CHCl_3$	442	98 ± 2	87–96[53,57–60]
Rhodamine B/ EtOH	552	98000 ± 2000	91400–117000[53, 61,62]
trans-Stilbene/ $CHCl_3$	302	26400 ± 300	28200–34000[53, 63–66]
$[Ni_2(cage)]^{2+}$/ MeCN	336	3090 ± 61	-

[a] Error calculated from the variability between three replicates, and the equipment and fitting uncertainties.

Continuous alteration methods can also be used to create continuous calibration curves with fixed analyte concentration but variation of other environmental conditions, such as pH, other species concentrations, or temperature. For alteration of pH or species concentrations, this would involve continuously adding a matrix solution containing a fixed analyte concentration to a solution containing the same fixed calibrant concentration and a species requiring modulation. This was demonstrated for bromophenol blue, a commonly used colorimetric pH indicator with useful range pH 3.0 (yellow) to pH 4.6 (blue) and pK_a 4.1 [70–72]. For this, acidic bromophenol blue solution (25.0 μM) was continuously added to a UV–Vis-monitored bromophenol blue conjugate base solution (25.0 μM, pH ~6.2), changing the matrix from blue to yellow and its pH from ~6.2 to ~2.3. The concentration of deprotonated bromophenol blue (λ_{max} ~592 nm) was estimated using a GAM-fitted continuous calibration curve (Fig. S9). In the pH-alteration continuous calibration, the bromophenol blue conjugate base concentration (25 μM) demonstrated a significant change (20 μM to 5 μM) between pH ~4.4 to ~3.4 corresponding with its useful range of pH 4.6–3.0 (Fig. 4). Furthermore, the acid and conjugate base forms of bromophenol blue were equally concentrated (12.5 μM) at pH 4.1, corresponding to a pK_a of 4.1 (Fig. 4). This demonstrated that calibration across a pH range could be performed in a single continuous calibration and suggested that monitoring the pH of a continuously calibrated system could allow rapid and precise elucidation of acid dissociation constants.

The experimental method and code were also applied to systems monitored with other characterization techniques. Continuous calibration was performed for reserpine and NaOAc calibrants monitored using MS and IR spectroscopy respectively (Fig. 5). The resultant MS calibration curve was similar in nature to those above, initially appearing linear but subsequently demonstrating non-linearity (Fig. 5A). Of the techniques investigated herein, MS is likely to benefit the most from improved calibration quality. This is due to its complex quantification and significant differences in calibration profiles for different analytes and experimental conditions, such as instrumentation. In contrast, the IR calibration curve demonstrated strong linearity, with the rainbow test

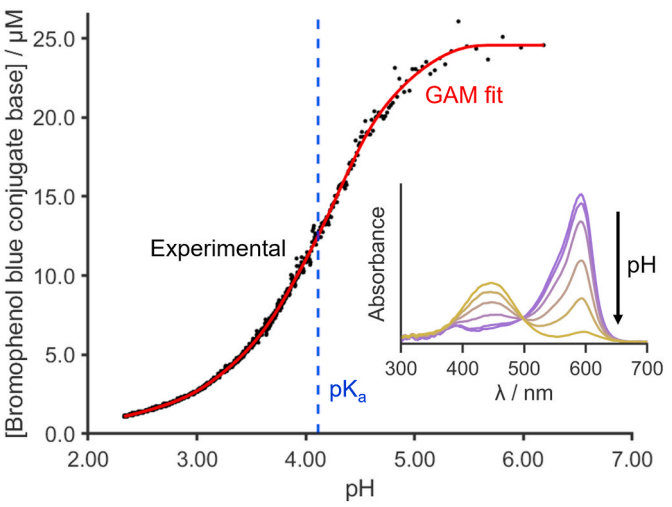

Fig. 4. Main) Continuous calibration curve of bromophenol blue (25 μM) across varying pH, monitored with UV–Vis spectroscopy, showing experimental data (black scatter) and the corresponding GAM fit (red line). At pH 4.1, the acid and conjugate base forms of bromophenol blue were equally concentrated (12.5 μM), corresponding to a pK_a of 4.1 (dashed blue line). Inset) Corresponding UV–Vis spectra between pH 5.5 and 2.5 at each pH 0.5 interval.

being passed at the maximum NaOAc concentration (Fig. 5B). This was likely due to minimal saturation occurring at the low absorbances observed for concentrated NaOAc solution. Nevertheless, the increased data density yielded through continuous calibration offers significantly higher precision than discrete calibration.

Continuous calibration was also used to improve the accuracy and precision of internal standardization. In internal standardization, a calibration curve should be used to relate analyte and internal standard intensities, which is usually approximated using a linear equation. However, slight differences in chemical properties between analyte and internal standard can cause non-linear deviations [1–3,8].

Continuous internal standardization calibration was performed using 1,10-phenanthroline as continuously added analyte (0–40 μM) in presence of 2,2′-bipyridine internal standard, monitored using MS. Internal standard was present in both the initial monitored solution and the addition solution to maintain its concentration (6.4 μM). This created a continuous calibration curve with fixed internal standard concentration but varied analyte concentration. Continuous addition of 1,10-phenanthroline caused the 2,2′-bipyridine corresponding peak intensity to decrease, likely due to suppression effects (Fig. 6A). Although the resultant analyte internal standard calibration curve was significantly more linear than the raw analyte calibration curve, it still demonstrated non-linearity (Fig. 6B). This highlighted the importance of collecting and applying such calibration curves for high accuracy internal standardization. As previously, these calibration curves were obtained with greater precision and speed using continuous calibration methods than possible with conventional discrete calibration. The fitted calibration curves can subsequently be applied to determine unknown analyte concentrations in samples with the same internal standard concentration.

4. Conclusions

The previously developed continuous calibration technique was simplified, expanded, and widely demonstrated, addressing its technical limitations and complexities. Simplification was implemented through modern accessible equipment, and an open-source code and a user-friendly web tool which streamlined data processing. The technique proved to be robust, showing high reproducibility and results that closely matched those obtained from conventional discrete calibrations. It was also demonstrated to be less time and labour intensive and much more precise than these discrete approaches, enabling more accurate linear and non-linear equations to be fitted than usually possible for such data-sparse methods.

The method was demonstrated across a wide range of analytical techniques, including external, standard addition, and internal standardization calibrations, as well as MS, and IR and UV–Vis spectroscopies. The latter of these generated molar absorption coefficients from a single experiment, with results for multiple analytes closely matching literature values. The technique was also demonstrated to be more efficient, precise, and robust than discrete calibration. Continuous calibration was extended to calibrate instrument response across pH ranges, yielding the literature pK_a of a weak acid from a single experiment.

We hope that the simplification, enhancement, and broad demonstration of continuous calibration will promote its adoption. The reduced time and labour intensity required by the method is hoped to not only accelerate calibration but also encourage scientists to conduct it more frequently. This, combined with the improved precision and accuracy offered by the method, will greatly improve experimental quality and reliability.

CRediT authorship contribution statement

Peter J.H. Williams: Writing – review & editing, Writing – original

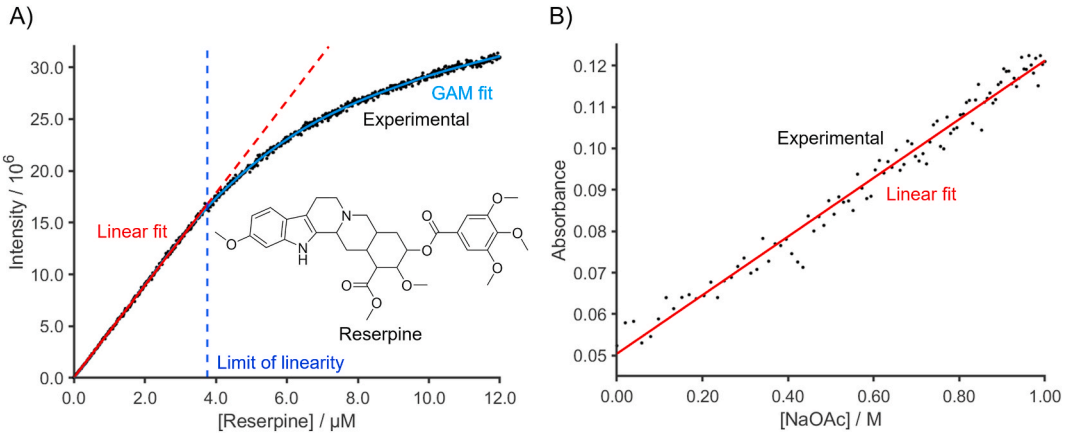

Fig. 5. Continuous calibration curves of A) reserpine monitored using MS and B) NaOAc monitored using IR spectroscopy. Depicted are experimental data (black scatter) and corresponding GAM (light blue line) and linear fits with algorithmically determined maximum limits of linearity (dashed dark blue line) which passed the rainbow test (solid red line), and continuation of the fits beyond the limits of linearity (dashed red line).

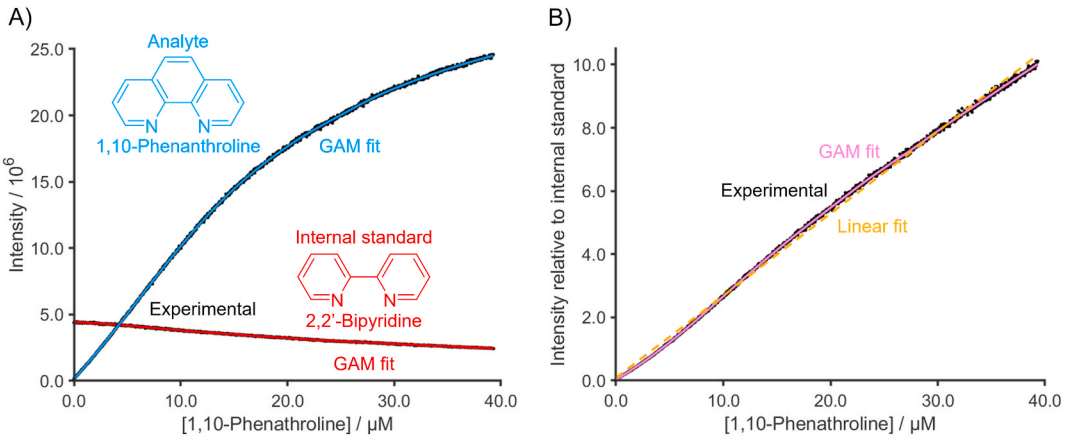

Fig. 6. A) Experimental continuous calibration (black scatter) and concave GAM fittings (coloured lines) of 1,10-phenanthroline analyte (light blue) in presence of 6.4 μM 2,2′-bipyridine internal standard (red) monitored by MS. B) Ratio of experimental (black scatter) and corresponding concave GAM-fitted (solid pink) analyte intensity to internal standard intensity showing deviation from linearity (dashed orange).

draft, Visualization, Software, Methodology, Investigation, Formal analysis, Conceptualization. **Nadini Thushara:** Methodology, Investigation. **Amin Yousefi:** Writing – review & editing, Writing – original draft, Methodology, Investigation. **Harrison Mundschutz:** Investigation. **Dennis K. Hore:** Writing – review & editing, Supervision, Funding acquisition. **J. Scott McIndoe:** Writing – review & editing, Supervision, Funding acquisition, Conceptualization.

Declaration of competing interest

The authors declare the following financial interests/personal relationships which may be considered as potential competing interests:J. Scott McIndoe reports financial support was provided by Natural Sciences and Engineering Research Council of Canada. If there are other authors, they declare that they have no known competing financial interests or personal relationships that could have appeared to influence the work reported in this paper.

Acknowledgements

We thank NSERC (Discovery and RTI programs) and the University of Victoria for operational and infrastructural support. We also thank Kavin Bhuvan for designing and optimizing the 3D-printed sample cell used for online IR measurements and Jack Smart and David Berg for providing the $[Ni_2(cage)]^{2+}$ complex.

Appendix A. Supplementary data

Supplementary data to this article can be found online at https://doi.org/10.1016/j.aca.2026.345285.

Data availability

The links to the code and data supporting this publication are provided in the manuscript file.

References

[1] L. Cuadros-Rodríguez, L. Gámiz-Gracia, E.M. Almansa-López, J.M. Bosque-Sendra, Calibration in chemical measurement processes. II. A methodological approach, TrAC, Trends Anal. Chem. 20 (2001) 620–636, https://doi.org/10.1016/S0165-9936(01)00111-X.

[2] L. Cuadros-Rodríguez, M.G. Bagur-González, M. Sánchez-Viñas, A. González-Casado, A.M. Gómez-Sáez, Principles of analytical calibration/quantification for the separation sciences, J. Chromatogr. A 1158 (2007) 33–46, https://doi.org/10.1016/j.chroma.2007.03.030.

[3] C. Stalikas, V. Sakkas, From a glimpse into the key aspects of calibration and correlation to their practical considerations in chemical analysis, Microchim. Acta 191 (2024) 81, https://doi.org/10.1007/s00604-023-06157-4.

[4] W.L. Cheng, C. Markus, C.Y. Lim, R.Z. Tan, S.K. Sethi, T.P. Loh, The IFCC working group on method evaluation protocols, calibration practices in clinical mass spectrometry: review and recommendations, Ann. Lab. Med. 43 (2023) 5–18, https://doi.org/10.3343/alm.2023.43.1.5.

[5] D.G. Blackmond, Reaction progress kinetic analysis: a powerful methodology for mechanistic studies of complex catalytic reactions, Angew. Chem. Int. Ed. 44 (2005) 4302–4320, https://doi.org/10.1002/anie.200462544.

[6] J.S. Mathew, M. Klussmann, H. Iwamura, F. Valera, A. Futran, E.A.C. Emanuelsson, D.G. Blackmond, Investigations of Pd-Catalyzed ArX coupling reactions informed by reaction progress kinetic analysis, J. Org. Chem. 71 (2006) 4711–4722, https://doi.org/10.1021/jo052409i.

[7] P.J.H. Williams, C. Killeen, I.C. Chagunda, B. Henderson, S. Donnecke, W. Munro, J. Sidhu, D. Kraft, D.A. Harrington, J.S. McIndoe, Continuous addition kinetic elucidation: catalyst and reactant order, rate constant, and poisoning from a single experiment, Chem. Sci. 14 (2023) 9970–9977, https://doi.org/10.1039/D3SC02698A.

[8] J.A. Carter, A.I. Barros, J.A. Nóbrega, G.L. Donati, Traditional calibration methods in atomic spectrometry and new calibration strategies for inductively coupled plasma mass spectrometry, Front. Chem. 6 (2018) 504, https://doi.org/10.3389/fchem.2018.00504.

[9] J. Martin, A.R. Gracia, A.G. Asuero, Fitting nonlinear calibration curves: no models perfect, J. Anal. Sci. Methods Instrum. 7 (2017) 1–17, https://doi.org/10.4236/jasmi.2017.71001.

[10] P.L. Urban, Quantitative mass spectrometry: an overview, Philos. Trans. R. Soc. Math. Phys. Eng. Sci. 374 (2016) 20150382, https://doi.org/10.1098/rsta.2015.0382.

[11] B.K. Matuszewski, M.L. Constanzer, C.M. Chavez-Eng, Strategies for the assessment of matrix effect in quantitative bioanalytical methods based on HPLC−MS/MS, Anal. Chem. 75 (2003) 3019–3030, https://doi.org/10.1021/ac020361s.

[12] P. Panuwet, R.E. Hunter, P.E. D'Souza, X. Chen, S.A. Radford, J.R. Cohen, M. E. Marder, K. Kartavenka, P.B. Ryan, D.B. Barr, Biological matrix effects in quantitative tandem mass spectrometry-based analytical methods: advancing biomonitoring, Crit. Rev. Anal. Chem. 46 (2016) 93–105, https://doi.org/10.1080/10408347.2014.980775.

[13] I. Omari, P. Randhawa, J. Randhawa, J. Yu, J.S. McIndoe, Structure, anion, and solvent effects on cation response in ESI-MS, J. Am. Soc. Mass Spectrom. 30 (2019) 1750–1757, https://doi.org/10.1007/s13361-019-02252-0.

[14] J. Liigand, A. Kruve, P. Liigand, A. Laaniste, M. Girod, R. Antoine, I. Leito, Transferability of the electrospray ionization efficiency scale between different instruments, J. Am. Soc. Mass Spectrom. 26 (2015) 1923–1930, https://doi.org/10.1007/s13361-015-1219-6.

[15] P.J.H. Williams, I.C. Chagunda, J.S. McIndoe, OptiMS: an accessible program for automating mass spectrometry parameter optimization and configuration, J. Am. Soc. Mass Spectrom. 35 (2024) 449–455, https://doi.org/10.1021/jasms.3c00354.

[16] I.C. Chagunda, P.J.H. Williams, T. Fisher, N.L. Stock, D.G. Beach, G.T. Thomas, J. Zhu, J.S. McIndoe, Comparative assessment of ESI-MS softness for inorganic complexes: how soft is your ESI-MS? Eur. J. Inorg. Chem. 27 (2024) e202400077 https://doi.org/10.1002/ejic.202400077.

[17] M. Defernez, R.H. Wilson, Infrared spectroscopy: instrumental factors affecting the long-term validity of chemometric models, Anal. Chem. 69 (1997) 1288–1294, https://doi.org/10.1021/ac961064o.

[18] F. Laborda, J. Medrano, J.R. Castillo, Influence of the number of calibration points on the quality of results in inductively coupled plasma mass spectrometry, J. Anal. At. Spectrom. 19 (2004) 1434, https://doi.org/10.1039/b408512d.

[19] M.T. Olson, A. Breaud, R. Harlan, N. Emezienna, S. Schools, A.L. Yergey, W. Clarke, Alternative calibration strategies for the clinical laboratory: application to

nortriptyline therapeutic drug monitoring, Clin. Chem. 59 (2013) 920–927, https://doi.org/10.1373/clinchem.2012.194639.
[20] O. Sonntag, T.P. Loh, Calibration – an under-appreciated component in the analytical process of the medical laboratories, Adv. Lab. Med. Av. En Med. Lab. 5 (2024) 148–152, https://doi.org/10.1515/almed-2023-0127.
[21] W. Xu, R.C. Sandford, P.J. Worsfold, A. Carlton, G. Hanrahan, Flow injection techniques in aquatic environmental analysis: recent applications and technological advances, Crit. Rev. Anal. Chem. 35 (2005) 237–246, https://doi.org/10.1080/10408340500323362.
[22] I.L. Garcia, P. Viñas, M.H. Córdoba, Calibration in flame atomic absorption spectrometry using a single standard and a gradient technique, J. Anal. Spectrom. 9 (1994) 553–561, https://doi.org/10.1039/JA9940900553.
[23] J.F. Tyson, J.M.H. Appleton, A continuous-dilution calibration technique for flame atomic-absorption spectrophotometry, Talanta 31 (1984) 9–14, https://doi.org/10.1016/0039-9140(84)80004-1.
[24] E. Paredes, S.E. Maestre, J.L. Todolí, A new continuous calibration method for inductively coupled plasma spectrometry, Anal. Bioanal. Chem. 384 (2006) 531–541, https://doi.org/10.1007/s00216-005-0169-4.
[25] E. Paredes, S.E. Maestre, J.L. Todolí, Use of stirred tanks for studying matrix effects caused by inorganic acids, easily ionized elements and organic solvents in inductively coupled plasma atomic emission spectrometry, Spectrochim. Acta Part B At. Spectrosc. 61 (2006) 326–339, https://doi.org/10.1016/j.sab.2006.03.005.
[26] K.L. Vikse, M.P. Woods, J.S. McIndoe, Pressurized sample infusion for the continuous analysis of Air- and moisture-sensitive reactions using electrospray ionization mass spectrometry, Organometallics 29 (2010) 6615–6618, https://doi.org/10.1021/om1008082.
[27] G.T. Thomas, S. Donnecke, I.C. Chagunda, J.S. McIndoe, Pressurized sample infusion, Chem. Mater. 2 (2022) e202100068, https://doi.org/10.1002/cmtd.202100068.
[28] C.R. Harris, K.J. Millman, S.J. Van Der Walt, R. Gommers, P. Virtanen, D. Cournapeau, E. Wieser, J. Taylor, S. Berg, N.J. Smith, R. Kern, M. Picus, S. Hoyer, M.H. Van Kerkwijk, M. Brett, A. Haldane, J.F. Del Río, M. Wiebe, P. Peterson, P. Gérard-Marchant, K. Sheppard, T. Reddy, W. Weckesser, H. Abbasi, C. Gohlke, T.E. Oliphant, Array programming with NumPy, Nature 585 (2020) 357–362, https://doi.org/10.1038/s41586-020-2649-2.
[29] W. McKinney, Data Structures for Statistical Computing in Python, Austin, Texas, 2010, pp. 56–61, https://doi.org/10.25080/Majora-92bf1922-00a.
[30] The pandas development team, pandas-dev/pandas: pandas. https://doi.org/10.5281/ZENODO.15831829, 2025.
[31] P. Virtanen, R. Gommers, T.E. Oliphant, M. Haberland, T. Reddy, D. Cournapeau, E. Burovski, P. Peterson, W. Weckesser, J. Bright, S.J. Van Der Walt, M. Brett, J. Wilson, K.J. Millman, N. Mayorov, A.R.J. Nelson, E. Jones, R. Kern, E. Larson, C. J. Carey, İ. Polat, Y. Feng, E.W. Moore, J. VanderPlas, D. Laxalde, J. Perktold, R. Cimrman, I. Henriksen, E.A. Quintero, C.R. Harris, A.M. Archibald, A.H. Ribeiro, F. Pedregosa, P. Van Mulbregt, , SciPy 1.0 Contributors, A. Vijaykumar, A. P. Bardelli, A. Rothberg, A. Hilboll, A. Kloeckner, A. Scopatz, A. Lee, A. Rokem, C. N. Woods, C. Fulton, C. Masson, C. Häggström, C. Fitzgerald, D.A. Nicholson, D. R. Hagen, D.V. Pasechnik, E. Olivetti, E. Martin, E. Wieser, F. Silva, F. Lenders, F. Wilhelm, G. Young, G.A. Price, G.-L. Ingold, G.E. Allen, G.R. Lee, H. Audren, I. Probst, J.P. Dietrich, J. Silterra, J.T. Webber, J. Slavič, J. Nothman, J. Buchner, J. Kulick, J.L. Schönberger, J.V. De Miranda Cardoso, J. Reimer, J. Harrington, J.L. C. Rodríguez, J. Nunez-Iglesias, J. Kuczynski, K. Tritz, M. Thoma, M. Newville, M. Kümmerer, M. Bolingbroke, M. Tartre, M. Pak, N.J. Smith, N. Nowaczyk, N. Shebanov, O. Pavlyk, P.A. Brodtkorb, P. Lee, R.T. McGibbon, R. Feldbauer, S. Lewis, S. Tygier, S. Sievert, S. Vigna, S. Peterson, S. More, T. Pudlik, T. Oshima, T.J. Pingel, T.P. Robitaille, T. Spura, T.R. Jones, T. Cera, T. Leslie, T. Zito, T. Krauss, U. Upadhyay, Y.O. Halchenko, Y. Vázquez-Baeza, SciPy 1.0: fundamental algorithms for scientific computing in python, Nat. Methods 17 (2020) 261–272, https://doi.org/10.1038/s41592-019-0686-2.
[32] F. Pedregosa, G. Varoquaux, A. Gramfort, V. Michel, B. Thirion, O. Grisel, M. Blondel, P. Prettenhofer, R. Weiss, V. Dubourg, J. Vanderplas, A. Passos, D. Cournapeau, Scikit-learn: machine learning in python, J. Mach. Learn. 12 (2011) 2825–2830.
[33] S. Seabold, J. Perktold, Statsmodels: econometric and statistical modeling with python, in: austin, Texas, 92–96, https://doi.org/10.25080/Majora-92bf1922-011, 2010.
[34] Charles F. Jekel, Gerhard venter, pwlf: a python library for fitting 1D continuous piecewise linear functions. https://github.com/cjekel/piecewise_linear_fit_py, 2019.
[35] Daniel Servén, Charlie Brummitt, Franz Király, JodesL, Alejandro Ouslan, Fräntz Miccoli, Joseph Egan IlyesD, Luc Lapenta, Lucas Servén Marín, Shushank Ranjan, Stephen Anthony Rose, Umberto Fasci, Viktor Szépe, hlink, Hassan Abedi, dswah/pyGAM: V0.10.1. https://doi.org/10.5281/ZENODO.16453423, 2025.
[36] The Matplotlib Development Team, Matplotlib: visualization with python. https://doi.org/10.5281/ZENODO.14436121, 2024.
[37] B. Dahlgren, ChemPy: a package useful for chemistry written in python, J. Open Source Softw. 3 (2018) 565, https://doi.org/10.21105/joss.00565.
[38] B. Dahlgren, ChemPy (2024), https://doi.org/10.5281/ZENODO.593188.
[39] J.M. Utts, The rainbow test for lack of fit in regression, Commun. Stat. Theor. Methods 11 (1982) 2801–2815, https://doi.org/10.1080/03610928208828423.
[40] O.Z. Devi, K. Basavaiah, K.B. Vinay, Application of potassium permanganate to spectrophotometric assay of metoclopramide hydrochloride in pharmaceuticals, J. Appl. Spectrosc. 78 (2012) 873–883, https://doi.org/10.1007/s10812-012-9547-9.
[41] S. Ganesh, F. Khan, M.K. Ahmed, P. Velavendan, N.K. Pandey, U.K. Mudali, Developed new procedure for low concentrations of hydrazine determination by spectrophotometry: hydrazine-potassium permanganate system, J. Anal. Sci. Methods Instrum. 2 (2012) 98–102, https://doi.org/10.4236/jasmi.2012.22018.
[42] K. Basavaiah, O. Zenita Devi, Application of oxidizing properties of permanganate to the determination of famotidine in pharmaceutical formulations, J. Mex. Chem. Soc. 54 (2010) 182–191, https://doi.org/10.29356/jmcs.v54i4.904.
[43] S.T. McBeath, D.P. Wilkinson, N.J.D. Graham, Analytical quantification of aqueous permanganate: direct and indirect spectrophotometric determination for water treatment processes, Chemosphere 251 (2020) 126626, https://doi.org/10.1016/j.chemosphere.2020.126626.
[44] R.M. Hassan, Prospective mechanistic on electron-transfer nature for reduction of permanganate ion by ascorbic acid in aqueous acidic solutions, J. Mol. Liq. 309 (2020) 113154, https://doi.org/10.1016/j.molliq.2020.113154.
[45] H.-P. Loock, P.D. Wentzell, Detection limits of chemical sensors: applications and misapplications, Sens. Actuators B Chem. 173 (2012) 157–163, https://doi.org/10.1016/j.snb.2012.06.071.
[46] M. Stüber, T. Reemtsma, Evaluation of three calibration methods to compensate matrix effects in environmental analysis with LC-ESI-MS, Anal. Bioanal. Chem. 378 (2004) 910–916, https://doi.org/10.1007/s00216-003-2442-8.
[47] J.T. Sloop, S.C. Allen, J.A. Carter, G.L. Donati, B.T. Jones, Matrix-matched two-point calibration based on the standard dilution analysis method, Microchem. J. 160 (2021) 105740, https://doi.org/10.1016/j.microc.2020.105740.
[48] J.T. Sloop, H.J.B. Bonilla, T. Harville, B.T. Jones, G.L. Donati, Automated matrix-matching calibration using standard dilution analysis with two internal standards and a simple three-port mixing chamber, Talanta 205 (2019) 120160, https://doi.org/10.1016/j.talanta.2019.120160.
[49] D.E. Bustos, R.E. Rivas, Standard dilution analysis (SDA) using high-resolution continuum source flame atomic absorption spectroscopy for the determination of Li, Cr, and Ni in complex matrices, Microchem. J. 212 (2025) 113470, https://doi.org/10.1016/j.microc.2025.113470.
[50] W.B. Jones, G.L. Donati, C.P. Calloway, B.T. Jones, Automated standard dilution analysis, J. Anal. At. Spectrom. 35 (2020) 178–187, https://doi.org/10.1039/C9JA00339H.
[51] W.B. Jones, G.L. Donati, C.P. Calloway, B.T. Jones, Standard dilution analysis, Anal. Chem. 87 (2015) 2321–2327, https://doi.org/10.1021/ac504152x.
[52] A.J. Ackroyd, L. Gajecki, A.T. Gogoulis, J.F. Smart, A.G. Oliver, J.S. McIndoe, D. J. Berg, Mausolates: large-cavity chelates with potential as delivery vehicles in nuclear medicine, Chem. Eur J. 30 (2024) e202401987, https://doi.org/10.1002/chem.202401987.
[53] M. Taniguchi, J.S. Lindsey, Database of absorption and fluorescence spectra of >300 common compounds for use in photochem CAD, Photochem. Photobiol. 94 (2018) 290–327, https://doi.org/10.1111/php.12860.
[54] D.J. Lougnot, P. Jacques, J.P. Fouassier, H.L. Casal, N. Kim-Thuan, J.C. Scaiano, New functionalized water-soluble benzophenones: a laser flash photolysis study, Can. J. Chem. 63 (1985) 3001–3006, https://doi.org/10.1139/v85-498.
[55] P. Kuś, P.G. Jones, Kuś jones 2000 synthesis of new tetraoxacyclophanes containing benzophenone units.pdf, Pol. J. Chem. 74 (2000) 965–977.
[56] G. Jancsó, Effect of D and 18O isotope substitution on the absorption spectra of aqueous copper sulfate solutions, Radiat. Phys. Chem. 74 (2005) 168–171, https://doi.org/10.1016/j.radphyschem.2005.04.011.
[57] A.N. Nesmeyanov, B.M. Yavorskii, G.B. Zaslavskaya, N.S. Kochetkova, Absorption spectra of some ferrocene derivatives, Dokl. Akad. Nauk SSSR 160 (1965) 837–840.
[58] R.E. Bozak, Photochemistry in the metallocenes, in: J.N. Pitts, G.S. Hammond, W. A. Noyes (Eds.), Adv. Photochem., first ed., Wiley, 1971, pp. 227–244, https://doi.org/10.1002/9780470133385.ch5.
[59] K.M. Roberts, M.A. Flahive, J.E. House, Thermodynamics of dissolution of ferrocene in n-octane, methanol, and acetonitrile, Polyhedron 53 (2013) 240–242, https://doi.org/10.1016/j.poly.2013.02.009.
[60] A. Paul, R. Borrelli, H. Bouyanfif, S. Gottis, F. Sauvage, Tunable redox potential, optical properties, and enhanced stability of modified ferrocene-based complexes, ACS Omega 4 (2019) 14780–14789, https://doi.org/10.1021/acsomega.9b01341.
[61] M. Beija, C.A.M. Afonso, J.M.G. Martinho, Synthesis and applications of rhodamine derivatives as fluorescent probes, Chem. Soc. Rev. 38 (2009) 2410, https://doi.org/10.1039/b901612k.
[62] A.G. Jadhav, S. Kothavale, N. Sekar, Red emitting triphenylamine based rhodamine analogous with enhanced Stokes shift and viscosity sensitive emission, Dyes Pigments 138 (2017) 56–67, https://doi.org/10.1016/j.dyepig.2016.11.021.
[63] R.N. Beale, E.M.F. Roe, 554. Ultra-violet absorption spectra of trans- and cis-stilbenes and their derivatives. Part I. trans- and cis-Stilbenes, J. Chem. Soc. (1953) 2755–2763, https://doi.org/10.1039/jr9530002755.
[64] F.D. Lewis, A.M. Bedell, R.E. Dykstra, J.E. Elbert, I.R. Gould, S. Farid, Photochemical generation, isomerization, and oxygenation of stilbene cation radicals, J. Am. Chem. Soc. 112 (1990) 8055–8064, https://doi.org/10.1021/ja00178a031.
[65] Á. Kvaran, Á.E. Konráðsson, C. Evans, J.K.F. Geirsson, 1 H NMR and UV–Vis spectroscopy of chlorine substituted stilbenes: conformational studies, J. Mol. Struct. 553 (2000) 79–90, https://doi.org/10.1016/S0022-2860(00)00546-9.
[66] H. Maeda, R. Horikoshi, M. Yamaji, T. Furuyama, M. Segi, Photophysical properties of silyl-substituted stilbene derivatives, Eur. J. Org. Chem. 2020 (2020) 3410–3422, https://doi.org/10.1002/ejoc.202000397.
[67] N.O. Mchedlov-Petrosyan, YuV. Kholin, Aggregation of rhodamine B in water, Russ. J. Appl. Chem. 77 (2004) 414–422, https://doi.org/10.1023/b:rjac.0000031281.69081.d0.
[68] S.M. Radiul, J. Chowdhury, S. Hazarika, Fluorescent H-aggregates of pure rhodamine B (RhB) in glycerol, ethylene glycol, methanol and butanol under

ambient condition, J. Mol. Struct. 1275 (2023) 134606, https://doi.org/10.1016/j.molstruc.2022.134606.
[69] J.S. Sandoval, B. Courtsal, A. Verma, D.W. McCamant, Excited state dynamics of Rhodamine B and its excitonically coupled dimer: a computational and experimental approach, J. Photochem. Photobiol. Chem. 455 (2024) 115756, https://doi.org/10.1016/j.jphotochem.2024.115756.
[70] F.Z. Henari, A. Al-Saie, K.G. Culligan, Optical limiting behavior of bromophenol blue and its dependence on pH, J. Nonlinear Opt. Phys. Mater. 21 (2012) 1250015, https://doi.org/10.1142/S0218863512500154.
[71] M. Chattopadhyaya, N.A. Murugan, Z. Rinkevicius, Origin of the absorption band of bromophenol blue in acidic and basic pH: insight from a combined molecular dynamics and TD-DFT/MM study, J. Phys. Chem. A 120 (2016) 7175–7182, https://doi.org/10.1021/acs.jpca.6b07660.
[72] A.A. Shalaby, A.A. Mohamed, Determination of acid dissociation constants of alizarin red S, methyl Orange, bromothymol blue and bromophenol blue using a digital camera, RSC Adv. 10 (2020) 11311–11316, https://doi.org/10.1039/C9RA10568A.